Quick XAFS Studies on the Y-Type Zeolite Supported Au Catalysts for $CO-O_2$ Reaction

Kazu Okumura,* Katsuhiko Yoshino, Kazuo Kato, and Miki Niwa

Department of Materials Science, Faculty of Engineering, Tottori University, Koyama-cho, Tottori 680-8552, Japan

Received: February 28, 2005; In Final Form: April 22, 2005

Au/zeolite catalysts prepared with a deposition−precipitation method were characterized with quick XAFS (QXAFS) in combination with IR. The data were correlated with the catalytic performance in the $CO-O_2$ reaction conducted at 273 K. On the basis of the XANES analysis of Au loaded on H−Y, the deposited Au_2O_3 was observed at the initial stage. The transformation of Au_2O_3 to form metal Au clusters was observed at 473 K in a H_2 atmosphere. The fact was supported by the IR measurement of adsorbed CO and the subsequent reaction with O_2. Detailed clustering process of Au supported catalysts could be directly followed by EXAFS analysis. The growth of metal Au proceeded via the formation of a Au_{55} cluster at 473 K. Then it agglomerated to give metal Au with diameter of 2 nm at 723 K. The addition of H_2 was effective to retard the sintering of Au clusters. A similar phenomenon was observed over Au loaded on USY zeolite. In marked contrast to the H−Y and USY supports, significantly agglomerated Au particles generated on Na−Y zeolite, indicating the importance of the presence of acid sites in keeping the Au clusters with highly dispersed form. The performance of 5 wt % Au loaded on H−Y and USY in the $CO-O_2$ reaction was remarkably sensitive to the pretreatment temperature and the gas atmosphere. The catalyst pretreated with hydrogen showed a two-spike pattern with respect to the pretreatment temperature. Namely, the optimum activity was observed after the pretreatment at 373 and 723 K, where the temperatures corresponded to the generation of Au_2O_3 and metal Au clusters with 2 nm diameter as evidenced by QXAFS analysis, respectively. The reason for enhancement of the activity of Au/H−Y by the addition of H_2 in the pretreatment step could be attributed to the formation of metal Au with appropriate size. In contrast to the H−Y and USY support, Au loaded on Na−Y prepared under the same condition was almost inactive in the reaction due to the formation of aggregated metal Au.

1. Introduction

Recently, growing interest has been devoted to supported gold catalysts since the pioneering work by Haruta et al.[1,2] This is because the catalysts exhibited unique catalytic performance in various reactions, including selective oxidation of CO in hydrogen, selective reduction of NO in the presence of O_2, and the epoxidation of propene.[3−8] Especially, CO oxidation conducted at low temperature has been extensively studied by many researchers. Deposition−precipitation was found to be one of the most effective methods for the preparation of highly active Au catalysts.[9,10] In the previous studies, reducible metal oxides, such as TiO_2 and Fe_2O_3, were preferably employed as supports for Au.[11] Recently, several research groups began to use zeolites as support for Au. For instance, Wan et al. reported that various conditions, such as temperature and the pH of the solution, affected the catalytic performance of Au.[12] Gates and co-workers tried to deposit Au complex on zeolites or MgO, and the catalysts were applied to the ethene hydrogenation.[13,14] Fraissard and co-workers used $Au(en)_2Cl_3$ complex to support the Au ions in the Y-type zeolites.[15−17] Salama et al. conducted the NO reduction by H_2 over Au^0 or Au(I) loaded on Na−Y zeolite.[18,19]

In the previous studies, the characterization of Au/zeolites has primarily been undertaken by means of TEM and XPS operated under high vacuum. However, in consideration of the nature of Au regarding the ready agglomeration of Au and the feasible reduction of Au oxides, the direct observation of Au clusters generated under in situ conditions was desired. To overcome the difficulty in characterizing the Au, we have tried to follow the reducing and growing process of Au using the quick XAFS (QXAFS) technique newly equipped in the Japan Synchrotron Radiation Research Institute (SPring-8). In the conventional XAFS measurement, a long time (10 min to 1 h) has been required to collect the data, since the monochromator was moved stepwise. On the other hand, the monochromator is moved continuously in the QXAFS measurement. As a result, the quick measurement, less than several seconds to minutes, becomes possible. The QXAFS technique combined with a brilliant X-ray source enables us to analyze the structure of Au under the in situ conditions in short measurement time. In particular, the direct characterization of Au with XAFS was important for the characterization of Au dispersed over zeolites. In the beginning of this study, we have prepared gold-supported FAU-type zeolites under different conditions. From the systematic studies concerning the loading of gold, the pH of the solution, and the temperature during the precipitation−deposition method, 5 wt % Au loaded on H−Y and USY zeolites prepared at pH 6 at 343 K for 1 h were found to be active in the $CO-O_2$ reaction. In the present study, QXAFS data in combination with IR spectra were correlated with the catalytic performance of Au. The experiment was carried out mainly through the comparison between Au loaded on H−Y and Na−Y. This study demonstrated how the results of detailed analysis were obtained by means of QXAFS technique.

* Corresponding author. E-mail: okmr@chem.tottori-u.ac.jp.

10.1021/jp051021o CCC: $30.25
Published on Web 06/03/2005

2. Experimental Section

2.1. Sample Preparation. FAU-type zeolites, i.e., Na−Y ($Si/Al_2 = 5.1$, Shokubai Kasei, Co.), H−Y ($Si/Al_2 = 5.5$, JRC-Z-HY5.5, The Catalysis Society of Japan), and USY ($Si/Al_2 = 7.51$, Shokubai Kasei, Co.), were employed as supports for Au. Au was loaded on these zeolites with a deposition−precipitation method. To 100 mL of $HAuCl_4$ (Wako Chemical Co.) solution heated in a water bath at 343 K was added 0.5 g of zeolite. The pH of the solution was adjusted at 6 by the addition of ammonia solution (2.8%) under vigorous stirring. The slurry continued to stir for an additional 1 h. After the filtration, the sample was thoroughly washed with deionized water until no Cl^- was detected with $AgNO_3$ solution. Finally, it was dried in air at 333 K for 3 h. The loading of Au was measured with ICP analysis after the digestion of Au/zeolite with HF solution, followed by dissolution with aqua regia. The loading of Au was determined to be 5 wt %.

2.2. QXAFS Measurement and Analysis. Quick XAFS measurements were performed at the BL01B1 in the SPring-8 with the approval of the Japan Synchrotron Radiation Research Institute (JASRI) (Proposal No. 2004B0311-NXa-np, 2005A0305-NXa-np). The storage ring was operated at 8 GeV. A Si(111) single crystal was used to obtain a monochromatic X-ray beam. Quick XAFS measurement of the Au L_3-edge was carried out in transmission mode. The Si(111) monochromator was moved from 10.0° to 8.7° in 1 min. The beam size was 1 × 5 mm at the sample position. The energy of X-ray was calibrated with Au foil as a reference. A self-supported wafer form of the sample (120 mg) with 7 mm diameter was placed in a quartz in situ cell. The sample was heated with a ramping rate of 5 K min^{-1} in a He flow (45 mL min^{-1}) or a 10% H_2 flow diluted with He (50 mL min^{-1}) under atmospheric pressure. The data of Au L_3-edge spectra were collected every 10 K.

For the extended X-ray absorption fine structure (EXAFS) analysis, the oscillation was extracted from the EXAFS data by a spline smoothing method.[20] The oscillation was normalized by edge height around 76 eV above the threshold. The Fourier transformation of the k^3-weighted EXAFS oscillation from k space to r space was performed over the range 30−130 nm^{-1} to obtain a radial distribution function. The inversely Fourier filtered data were analyzed with a usual curve fitting method. The empirical phase shift and amplitude functions for Au−Au were extracted from the data for Au foil measured at the same temperature. The curve fitting analysis was initiated with the use of Debye−Waller factors extracted from EXAFS spectra of Au foil measured at the same temperatures. The Debye−Waller factors of Au foil at higher temperatures were determined on the basis of the spectrum of Au foil measured at room temperature. Errors for coordination number and bond distance were estimated to be 10% and 0.001 nm, respectively. The uncertainty in the analysis defined by eq 1 (R factor) was 0.1−1.5%.

$$R_f = \int |k^3\chi^{obs}(k) - k^3\chi^{calc}(k)|^2 \, dk / \int |k^3\chi^{obs}(k)|^2 \, dk \quad (1)$$

2.3. IR Measurement. IR spectra were measured with the Parkin-Elmer Spectrum One spectrometer. The spectra were recorded with a 4 cm^{-1} resolution. A self-supported wafer with 10 mm diameter (9 mg) was placed in a quartz in situ cell. The sample was pretreated in a 6% H_2 flow diluted with Ar at 373 or 723 K. After cooling to the room temperature, CO (1.0 kPa) was admitted to the pretreated sample, followed by evacuation of CO gas. Then O_2 (21 kPa) was admitted to the in situ cell. The IR spectra were recorded in each step at room temperature. The difference spectra were obtained after subtracting the spectrum of pretreated Au/H−Y from those of samples exposed to CO or O_2.

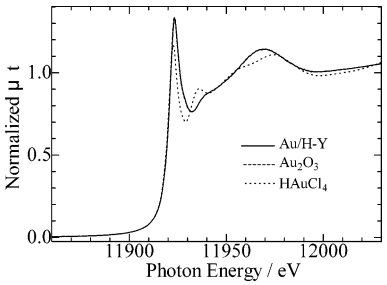

Figure 1. Au L_3-dge XANES spectra of 5 wt % as-made Au/H−Y, Au_2O_3, and $HAuCl_4$.

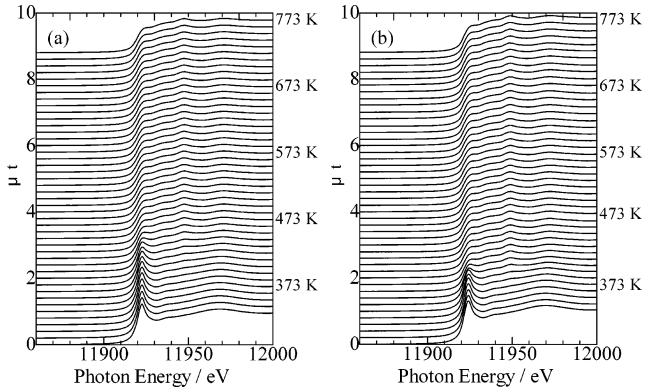

Figure 2. Au L_3-edge XANES of 5 wt % Au loaded on (a) H−Y and (b) Na−Y zeolite measured in a 10% H_2 flow. Temperature ramping rate, 5 K min^{-1}.

2.4 Catalytic Reaction. CO−O_2 reaction was carried out with a fixed-bed flow reactor. A 0.1 g portion of Au/zeolite (60−80 mesh) mounted in a Pyrex glass reactor was pretreated with 10% H_2 (N_2 balance, 30 mL min^{-1}) or N_2 (30 mL min^{-1}) at different temperatures for 0.5 h. The catalyst was cooled to 273 K using an ice bath prior to the reaction. A gas mixture of 1% CO and 20% O_2 diluted with N_2 was fed into the catalyst under atmospheric pressure. The total flow rate was 33 mL min^{-1}. The effluent gas was analyzed with a gas chromatograph equipped with a TCD detector. Molecular Sieves 13X and Porapak Q columns were used to separate the gas mixture. The CO conversion was measured after 10 min from the admission of a CO−O_2 gas mixture when the flowing rate of gas was stabilized.

3. Results

3.1. XANES Data Analysis. Figure 1 gives the Au L_3-edge XANES spectra of Au_2O_3, $HAuCl_4$, and as-made 5 wt % Au/H−Y. As can be seen from the figure, the spectra of Au_2O_3 and Au/H−Y were closely similar, implying the formation of Au_2O_3 on H−Y in the incipient sample. However, the XANES spectrum of Au/H−Y was considerably different from that of $HAuCl_4$. For instance, the characteristic peak that appeared at 11 936 eV in the spectrum of $HAuCl_4$ was not observed in that of Au/H−Y, indicating that the Au−Cl bond was completely removed during the preparation of Au/H−Y. The fact was confirmed on the basis of the EXAFS spectra, as will be mentioned later.

Figure 2 displayed the Au L_3-edge XANES spectra of Au/H−Y and Na−Y measured during temperature programmed reduction in 10% H_2. The intense white line at 11 923 eV characteristic of Au_2O_3 could be seen in the beginning of the

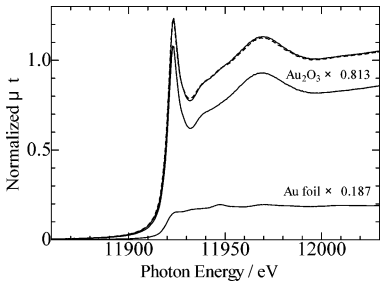

Figure 3. XANES spectrum of 5 wt % Au/H−Y at 393 K measured in 10% H_2 and the linear combination of weighted XANES spectra of Au foil and Au_2O_3 (dotted line).

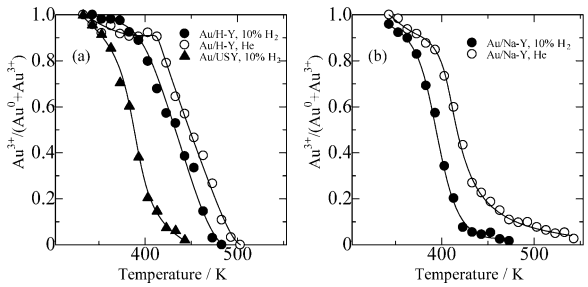

Figure 4. $Au^{3+}/(Au^{3+} + Au^0)$ ratio determined from XANES spectra of (a) Au/H−Y and Au/USY, and (b) Au/Na−Y in an atmosphere of 10% H_2 or He. Au loading, 5 wt %.

experiment. The appearance of the white line originated from the $2p_{3/2} \rightarrow 5d$ transition. On raising the temperature, the intensity of the white line gradually decreased due to the reduction of Au_2O_3 to form Au^0. The complete transformation from Au_2O_3 to Au^0 took place at around 473 and 423 K over H−Y and Na−Y supports, respectively. To determine the relative concentration of metal Au and Au oxides, Au L_3-edge XANES spectra were fitted with the combination of the spectra for Au foil and Au_2O_3 using a least-squares method. Figure 3 displays an example of fitted data of Au/H−Y treated with H_2 at 393 K. We confirmed that the quantitative fitting of the spectrum was achieved enough to calculate the ratio of Au^{3+} and Au^0. The calculated ratios of Au^{3+} and the total amount of Au were summarized in Figure 4. It was obvious to see that the Au^{3+} phase was stable at the lower temperature region. For example, the Au^{3+} present in Au/H−Y treated at 373 K in 10% H_2 was calculated to be 98% (Figure 4a, ●). On increasing the temperature, the ratio of Au^{3+} decreased and Au was completely reduced to Au^0 at 483 K. When the measurement was carried out in a He flow, the curve shifted to the higher temperature by 20 K, meaning that the reduction of Au_2O_3 was promoted by the addition of H_2. In the case of Au loaded on USY measured in 10% H_2, the reduction of Au progressed at lower temperature than that of Au/H−Y, where 70% of the total Au remained as Au_2O_3 at 373 K (Figure 4a, ▲). The reduction of Au^{3+} ratio progressed with a single step, suggesting the homogeneous distribution of the size of Au over H−Y or USY zeolites.

The change of Au^{3+} ratio over Au/Na−Y was different from that of Au/H−Y or USY, i.e., the reduction of Au/Na−Y proceeded with double steps (Figure 4b). Namely, after the steep decrease in $Au^{3+}/(Au^{3+} + Au^0)$ ratio, a slow reduction step was observed above 423 and 453 K in 10% H_2 and He, respectively. Probably, the appearance of the slow reduction step suggested the presence of bulky Au_2O_3 or a heterogeneous distribution of Au_2O_3 with different size.

3.2. EXAFS Analysis. Parts a and b of Figure 5 give the EXAFS $k^3\chi(k)$ spectra and their Fourier transforms for Au_2O_3, $HAuCl_4$, and as-made 5 wt % Au/H−Y, respectively. Apparently, the spectra of Au_2O_3 and Au/H−Y were closely similar, whereas they were considerably different from the spectrum of $HAuCl_4$. The fact was confirmed from both $k^3\chi(k)$ spectra and their Fourier transforms. The data obviously indicated the deposition of Au_2O_3 as already evidenced by XANES spectra.

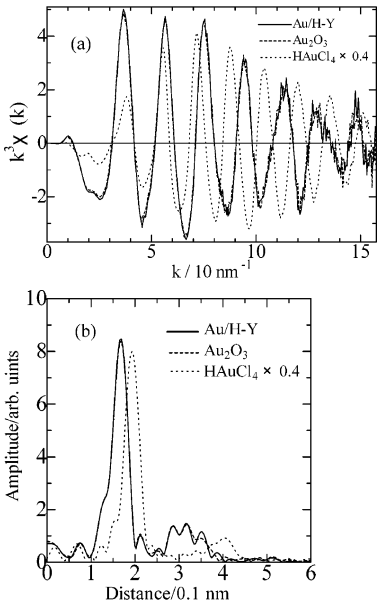

Figure 5. Au L_3-edge (a) $k^3\chi(k)$ spectra, and (b) their Fourier transforms of as-made 5 wt % Au/H−Y, Au_2O_3, and $HAuCl_4$.

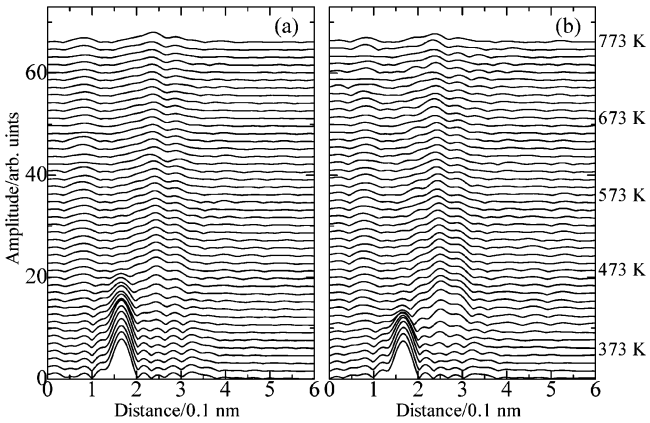

Figure 6. Au L_3-edge EXAFS Fourier transform of 5 wt % Au loaded on (a) H−Y and (b) Na−Y zeolite measured in 10% a H_2 flow. Fourier transform range, 30−130 nm^{-1}. Temperature ramping rate, 5 K min^{-1}.

Representative Fourier transforms of the $k^3\chi(k)$ EXAFS for Au-loaded H−Y and Na−Y are given in Figure 6. The peak appearing at 0.18 nm (phase shift uncorrected) could be assigned to the Au−O bond from the comparison with that of Au_2O_3 (Figure 5b). Accompanied by raising the temperature, the intensity of the Au−O bond decreased. Alternatively, a broad peak appeared at 0.18−0.33 nm. The peak was assigned to the Au−Au bond of metal Au. Such a transformation from Au_2O_3 to metal Au agreed well with the analysis of XANES spectra given in Figure 4. Due to the small size of the generated Au clusters, no other shell beyond the first one could be seen in the Fourier transforms of Au/H−Y.

The coordination number (CN) of the nearest neighboring Au−Au bond of metal Au was calculated on the basis of the curve-fitting analysis. The data of CNs over Au/H−Y and USY are displayed in Figure 7a. In the case of Au/H−Y measured in 10% H_2, the CN rapidly increased up to 473 K (Figure 7a, ●). The steep increase of CN meant the reduction of Au_2O_3 to

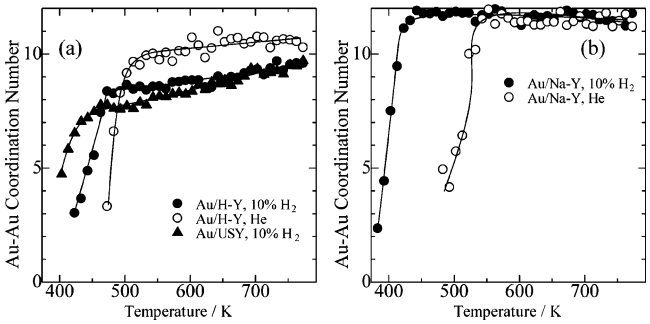

Figure 7. Dependence of nearest neighboring Au−Au coordination number on the temperature determined from Au L_3-edge EXAFS of (a) Au/H−Y, USY, and (b) Au/ Na−Y in an atmosphere of 10% H_2 or He. Au loading, 5 wt %.

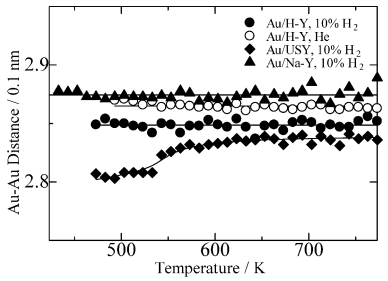

Figure 8. Dependence of nearest neighboring Au−Au interatomic distance on the temperature determined from Au L_3-edge EXAFS of 5 wt % Au loaded on H−Y, USY, and Na−Y.

form metal Au, because the intensity of the Au−O bond decreased simultaneously at the same temperature range (Figure 6a). After completion of the reduction at 473 K, the CN reached to 8.2. Then the CN gradually increased with increase in the temperature. A similar change in CN of the Au−Au bond was observed on Au/USY (Figure 7a, ▲), although it was slightly lower than that of Au/H−Y. The change in CN of Au/H−Y measured in a He flow was different from that measured in 10% H_2 (Figure 7a, ○). That is to say, the CN rapidly increased to 9.7 at 513 K, accompanied by desorption of oxygen from Au_2O_3, and the value gradually increased with an increase in the temperature. From the comparable experiments conducted in the different gas atmosphere, it could be noted that smaller Au clusters was remained by the addition of H_2, considering that the CN measured in a 10% H_2 flow was smaller than that in a He flow.

Figure 7b gives the CN of nearest neighboring metal Au−Au bond of Au/Na−Y. The CN rapidly increased up to 443 and 553 K in an atmosphere of 10% H_2 or He flow, respectively. The change meant the reduction of Au_2O_3 to give metal Au in a similar manner as the Au/H−Y and USY. However, it could be seen that the CN of the Au−Au bond already reached to 11.5 accompanied by the completion of the reduction. The CN did not change on further raising the temperature. In the case of bulk Au (Au foil), each Au atom is surrounded by 12 Au atoms forming a close-packed structure. Therefore, the CN of Au−Au bond observed on Na−Y was close to the CN = 12 of bulk metal Au in the fcc lattice, meaning the generation of a highly aggregated metal Au on Na−Y.

Figure 8 displays the Au−Au interatomic distance of metal Au generated in H−Y, USY, and Na−Y supports determined with curve-fitting analysis. The distance of Au/Na−Y and Au/H−Y (in He) was calculated to be 0.287 and 0.286 nm, respectively. The value was close to that of Au foil (0.2884 nm). In the case of Au/H−Y and USY, the Au−Au distance measured in the atmosphere of 10% H_2 was calculated to be

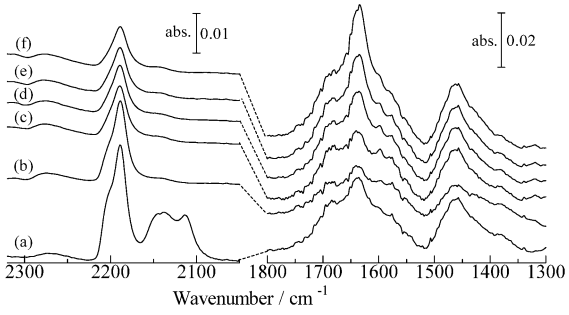

Figure 9. FTIR spectra of 5 wt % Au/H−Y pretreated at 373 K in 6% H_2: (a) after exposure to 1.0 kPa of CO (the spectrum of gaseous CO was subtracted), (b) after evacuation of CO, (c−f) after the admission of 21 kPa of O_2 measured every 8 min. The spectra were subtracted from that of pretreated sample. Measurements were carried out at room temperature.

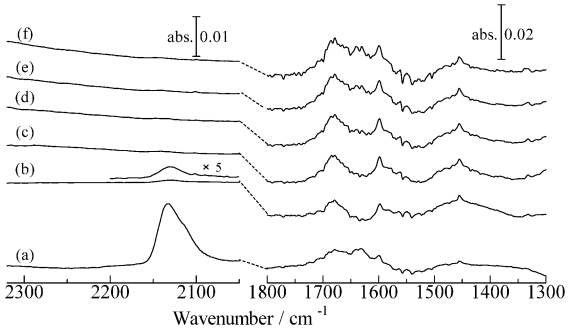

Figure 10. FTIR spectra of 5 wt % Au/H−Y pretreated at 723 K in 6% H_2: (a) after exposure to 1.0 kPa of CO (the spectrum of gaseous CO was subtracted), (b) after evacuation of CO, (c−f) after the admission of 21 kPa of O_2 measured every 8 min. The spectra were subtracted from that of pretreated sample. Measurements were carried out at room temperature.

0.285 nm and 0.280−0.284 nm, respectively, which was notably shorter than that observed on Au/Na−Y, H−Y in He.

3.3. IR Spectra of Au/H−Y. IR spectra of adsorbed CO and subsequent reaction with O_2 were measured over Au/H−Y pretreated at 373 and 723 K in a 6% H_2 flow (Figures 9 and 10). The temperatures corresponded to the generation of Au_2O_3 and metal Au as proved by QXAFS analysis, respectively. In these figures, the difference spectra of CO-adsorbed Au/zeolite and pretreated ones were displayed. After the exposure of 1.0 kPa of CO over Au/H−Y pretreated at 373 K, adsorbed CO bands appeared at 2113, 2139, 2189, 2204, and 2274 cm^{-1} (the spectrum of CO in gas phase was subtracted). On evacuation of the gaseous CO, the peaks at 2113 and 2139 cm^{-1} diminished, while an intense band at 2189 cm^{-1}, a shoulder at 2204 cm^{-1}, and a weak band at 2274 cm^{-1} remained. After the subsequent admission of 21 kPa of O_2, the intensity of the strong peak at 2189 cm^{-1} and a shoulder at 2204 cm^{-1} decreased, whereas a small peak at 2274 cm^{-1} remained unchanged with the duration of time. On the other hand, several peaks ascribed to the carbonate or bicarbonate were already observed between 1350 and 1700 cm^{-1} (carbonate region) after the exposure of 1.0 kPa CO. The intense peaks observed around 1640 and 1460 cm^{-1} were assigned to the bicarbonates.[21−23] Probably, the peak at 1640 cm^{-1} was overlapped with the deformation band of adsorbed H_2O. The bands that appeared at 1685 and 1585 cm^{-1} were tentatively assigned to the bidentate species of carbonate.[24,25] After the evacuation of CO and the subsequent admission of 21 kPa of oxygen, the intensity of the carbonate and bicarbonate species increased with duration time, accompanied by the reduction of the linearly adsorbed CO bands at 2189 and 2204 cm^{-1}. Especially, the vibrations at 1640 and

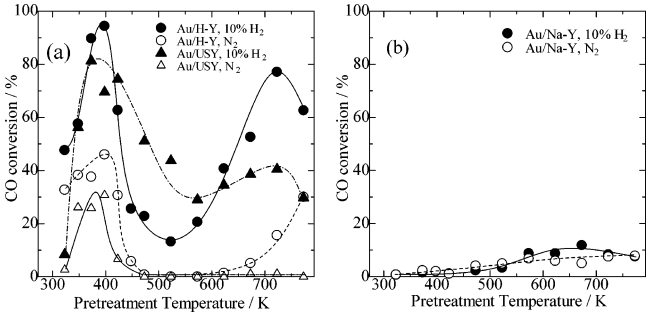

Figure 11. Dependence of the initial $CO-O_2$ conversion on the pretreatment temperature in the atmosphere of N_2 and 10% H_2. (a) Au/H−Y and Au/USY, (b) Au/Na−Y. Au loading, 5 wt %; reaction temperature, 273 K; CO, 1%; O_2, 20%; total flow rate, 33 mL min^{-1}.

1460 cm^{-1}, which were ascribed to the bicarbonate, developed with duration of time. The simultaneous change suggested that the linearly adsorbed CO reacted with O_2 to give CO_2, and the generated CO_2 adsorbed on the surface of Au_2O_3.

Different features in IR spectra were observed over Au/H−Y pretreated at 723 K, as displayed in Figure 10. After the admission of 1.0 kPa of CO, an intense peak appeared at 2133 cm^{-1}, accompanied by a shoulder at 2113 cm^{-1}. These peaks may be assigned to the linearly adsorbed CO on the metal Au surface. The peaks almost diminished after the evacuation of the gaseous CO, and only a small one remained at 2129 cm^{-1}. The peak at 2129 cm^{-1} disappeared completely after the exposure of 21 kPa of O_2. The bands due to the carbonate and bicarbonate appeared between 1700 and 1350 cm^{-1}. The intensity of these bands increased with duration time after the admission of O_2. Therefore, the linearly adsorbed CO (2129 cm^{-1}) appeared to be an active species for the $CO-O_2$ reaction. The intensity of the adsorbed CO and the growing extent of these peaks were lower than that observed on Au/H−Y pretreated at 373 K. The differences in the features of the IR spectra suggested the generation of different Au species depending on the pretreatment temperature.

3.4. Catalytic Performance of Au-Loaded Zeolites. Figure 11 shows the conversion of CO in the $CO-O_2$ reaction plotted as a function of pretreatment temperature. It was obvious that the catalytic performance of Au loaded on H−Y and USY was significantly sensitive to the pretreatment temperature (Figure 11a). That is to say, they exhibited a two-spike pattern with respect to the pretreatment temperature at 373 and 723 K. As for the effect of gas in the pretreatment step, the catalytic activity was enhanced by the addition of H_2 in the pretreatment.

In marked contrast to the Au/H−Y and Au/USY, the activity of Au/Na−Y was quite low, regardless of the temperature and the kind of flowing gas in the pretreatment (Figure 11b). Therefore, it was noted that the presence of acid sites played an important role in the generation of active Au species over Y-type zeolite.

4. Discussion

The change in the oxidation state and the growing process of Au clusters were successfully followed by in situ QXAFS analysis. From the close similarity in the XANES as well as EXAFS data between authentic Au_2O_3 and Au/Y-zeolite, Au_2O_3 was proved to be loaded on H−Y at the initial stage. The Au_2O_3 was almost preserved, even after the treatment at 373 K in 10% H_2. The temperature corresponded to the first maxima in the $CO-O_2$ reaction over Au/H−Y (Figure 11a). Therefore, the predominant active Au species of the first peak could be assigned to the Au_2O_3 or partially reduced Au oxide. This fact was consistent with the IR spectra. After the admission of CO and subsequent evacuation, an intense peak appeared at 2189 cm^{-1}, accompanied by a shoulder at 2204 cm^{-1}. These peaks were considered to be active species in the $CO-O_2$ reaction from the simultaneous change observed after the exposure of O_2. In the literature, CO adsorbed on metal Au surfaces was observed between 2060 and 2130 cm^{-1}.[26−28] On the other hand, CO on the positively charged Au was reported to appear at higher wavenumber compared with that on Au^0. Lee et al. observed an adsorbed CO band at 2175 cm^{-1} on the unreduced Au catalyst.[29] Ichikawa's group observed bands at 2170 and 2186 cm^{-1} for CO adsorbed on Au^+ loaded on ZSM-5 and NaY, respectively.[30,31] Boccuzzi et al. reported the CO adsorbed on oxidic Au species at 2176 cm^{-1}.[32] The shift of the CO stretching band to higher wavenumumber over Au^{n+} was explained through the wreaking of the back-donation of metal to the $2\pi^*$ antibonding orbital of CO. The wavenumbers of CO species observed at 2189 and 2204 cm^{-1} on Au/H−Y (373 K) was obviously higher than that of CO adsorbed on Au^0, whereas the values were close to the positively charged Au^{n+} reported in the literature. Therefore, it was supposed that the CO adsorbed on Au_2O_3 or partially reduced Au^{n+} participated in the $CO-O_2$ reaction. The adsorbed CO appeared at 2189 cm^{-1} and remained unchanged, even after the evacuation of gaseous CO, indicating the strong interaction between CO and the surface of cationic Au. On the other hand, the bands at 2113 and 2139 cm^{-1} may be assigned to the CO adsorbed on metal Au^0, which was generated through the reaction of Au_2O_3 with CO. This is because the CO adsorption bands appeared over Au^0 at the same positions (Figure 10), and the wavenumbers were close to those observed in the literature as cited above. In addition, the peaks readily disappeared through the evacuation of the gas phase, as similarly observed over Au^0. Although the peak that appeared at 2274 cm^{-1} was not clearly assigned, this may be due to the adsorption on Au^{3+}, considering that the wavenumber was higher than that of Au^+-CO (2189 and 2204 cm^{-1}). In the studies of CO adsorption on zeolites, CO interacted with acidic OH groups that were observed at 2172 cm^{-1}.[33] However, the CO adsorption was observed only at low temperature, due to the weak interaction. In agreement with the report, the adsorbed CO was not observed on H−Y measured at room temperature. Therefore, the adsorption of CO was confirmed to take place on the surface of Au.

The Au loaded on zeolites treated at higher temperature was assigned to Au^0 as evidenced by XANES as well as EXAFS analysis. The fact was consistent with the IR spectra measured after the admission of CO and subsequent evacuation. On exposure of 1.0 Pa CO, an adsorbed CO appeared at 2129 cm^{-1}, which agreed with the reported wavenumber of linearly adsorbed CO on the metal Au encaged in H−Y zeolite.[34] The peak almost disappeared immediately after evacuation. The behavior also agreed with the characteristics of CO on the metal Au, since adsorption of CO on metal gold surface was generally reversible at room temperature.[34] In consideration of these data, the active species for $CO-O_2$ reaction in the second peak in Figure 11a (723 K) could be attributed to the Au^0. The temperature for reduction of Au observed here (around 473 K) agrees well with that reported previously. Namely, Chang et al. showed that the reduction of AuO_x species took place at 453 K.[35] In the TPR studies of the bulk Au_2O_3, Venugopal et al. observed the reduction peaks at 468 and 505 K, which corresponded to the reduction of Au_2O_3 to AuO and AuO to Au, respectively.[36]

When the reduction of Au_2O_3 was completed at 473 K over H−Y in a 10% H_2 flow, the CN of Au−Au reached to 8.2.

Similarly, the CN of metal Au reached to 7.8 over USY support at 473 K. Assuming the cuboctahedron structure, the CNs were close to that of a Au cluster composed of 55 Au atoms (CN = 7.8), corresponding to the two-shell structure of a cuboctahedron (13 + 42 atoms). The diameter of the Au_{55} cluster could be estimated to be 1.3 nm. The size agreed well with the pore diameter of the supercage of FAU-type zeolite. Thus, the formation of Au_{55} clusters in the supercage as well as on the external surface of Y-type zeolites was inferred. The formation of Au clusters was consistent with the fact that the nearest neighboring Au−Au distance of Au/H−Y, USY was shorter than that of bulk Au or aggregated Au generated on Na−Y (Figure 8). The tendency agreed with the Au−Au bond distance of Au_{55} clusters determined on the basis of the EXAFS analysis.[37] Thus, the nearest neighboring Au−Au interatomic distance of $Au_{55}(PPh_3)_{12}Cl_{16}$, $Au_{55}(T_8{-}OSS{-}SH)_{12}Cl_{16}$, and $Au_{55}(PPh_3)_{12}Cl_{16}$ in Al_2O_3 was determined to be 0.2794, 0.2785, and 0.284 nm, respectively. On subsequently raising the temperature, the CN gradually increased and the value reached to 9.5 at 723 K, corresponding to the second peak in the CO−O_2 reaction (Figure 11a). From the CN value, the size of the Au clusters was estimated to be 2 nm, assuming the cuboctahedron structure.[38] Apparently, the size was larger than that of the supercage of FAU zeolite. Hence, it was supposed that the agglomeration of Au_{55} clusters progressed on the external surface of H−Y and USY zeolites. In the studies on TiO_2 support, the optimum gold particle size was found to be 2−3 nm.[39,40] The size coincided with that of active Au^0 loaded on H−Y or USY in the present study.

From the comparison of the CN changes between the atmosphere of 10% H_2 and the He flow, the effect of the H_2 was revealed. Namely, the agglomeration of Au was suppressed by the addition of H_2. Although the role of H_2 is not clear at this stage, one possibility is that the formation of Au−H complex promoted the migration of Au onto the acid sites of zeolites. In a manner similar to the hypothesis, it has been reported that the addition of H_2 promoted the mobility of Pt due to the formation of Pt−H complexes on the single crystal of Pt.[41]

The manner of growing of Au on Na−Y zeolite was significantly different from that of Au/H−Y and USY. That is to say, the formation of highly aggregated metal Au was observed on Na−Y. The large size of Au may be attributed to the reason for the low activity of Au/Na−Y in the CO−O_2 reaction (Figure 11b). In the light of the difference in the behavior between H−Y and Na−Y, it was supposed that acid sites of Y-type zeolite played an important role in generation of well-dispersed Au metal. The effect of an acid site was also reported by Fraissard et al. They illustrated that the smaller Au clusters were prepared over acidified Y-type zeolite in comparison with Na−Y zeolite.[42] Moreover, it was found that higher acidified zeolite (Na,H−Y) showed greater stability under O_2.[17] Wan et al. indicated that the surface treatment of Y-type zeolite was important to obtain the Au-loaded catalysts with high activity where the small and uniform Au was distributed.[43] Two hypotheses could be considered to explain the effect of Brønsted acid sites observed here. The first one is the influence of acid site in the preparation step. In the deposition−precipitation method, the pH of the aqueous solution of $HAuCl_4$ was adjusted with ammonia to give deposited $Au(OH)_3$. In consideration of the basic character of $Au(OH)_3$, the interaction of $Au(OH)_3$ and acid sites of H−Y promoted the formation of dispersed Au species. After the thorough washing and drying at 333 K, the formation of Au_2O_3 was observed. Probably, the initially deposited $Au(OH)_3$ was dehydrated to give Au_2O_3 in the drying step or acid sites functioned as catalyst for polymerization of $Au(OH)_3$ to form Au_2O_3, as proposed by Wan et al.[43] The other possibility is that the strong interaction between metal Au and Brønsted acid sites kept the dispersed metal Au clusters, as explained by Fraissard et al.[42] In analogy with the effect of acid sites, the stabilization of small Au particle was achieved in the presence of OH groups on supports. The fact was clearly evidenced with Au/$Fe(OH)_3$ that was extremely active in the CO−O_2 reaction at low temperature.[44] Similar phenomena were also found on Pd loaded on zeolites, where the selective formation of Pd_6 or Pd_{13} clusters was found on H−Mordenite or H−ZSM-5 and H−Y zeolites, respectively.[45]

5. Conclusions

Au loaded on various kinds of zeolite was characterized by means of QXAFS in combination with IR spectra, and the data were related with the catalytic performance. Au_2O_3 was initially deposited on H−Y (USY) after the preparation of the catalyst by the precipitation−deposition method. The Au_2O_3 transformed to agglomerated Au^0 via the formation of Au_{55} clusters. The initially deposited Au_2O_3 or partially reduced Au oxide and Au^0 with 2 nm diameter were considered to be active species after pretreatment at 373 and 723 K. The agglomeration of Au was suppressed by the addition of H_2. Probably, this is the reason for the positive effect of the addition of H_2 in the pretreatment step. Contrary to the H−Y and USY supports, remarkably aggregated Au^0 was generated over the Na−Y support, leading to the low activity in the CO−O_2 reaction.

References and Notes

(1) Haruta, M.; Yamada, Y.; Kobayashi, T.; Iijima, S. *J. Catal.* **1989**, *115*, 301.
(2) Haruta, M. *Catal. Today* **1997**, *36*, 153.
(3) Sanchez, R. M. T.; Ueda, A.; Tanaka, K.; Haruta, M. *J. Catal.* **1997**, *168*, 125.
(4) Ueda, A.; Oshima, T.; Haruta, M. *Appl. Catal. B* **1997**, *12*, 81.
(5) Kalvachev, Y. A.; Hayashi, T.; Tsubota, S.; Haruta, M. *J. Catal.* **1999**, *186*, 228.
(6) Hayashi, T.; Tanaka, K.; Haruta, M. *J. Catal.* **1998**, *178*, 566.
(7) Jia, J. F.; Haraki, K.; Kondo, J. N.; Domen, K.; Tamaru, K. *J. Phys. Chem. B* **2000**, *104*, 11153.
(8) Haruta, M.; Daté, M. *Appl. Catal. A, Gen.* **2001**, *222*, 427.
(9) Tsubota, S.; Cunningham, D. A. H.; Bando, Y.; Haruta, M. *Stud. Surf. Sci. Catal.* **1995**, *91*, 227.
(10) Zanella, R.; Giorgio, S.; Shin, C.-H.; Henry, C. R.; Louis, C. *J. Catal.* **2004**, *222*, 357.
(11) Yuan, Y.; Asakura, K.; Wan, H.; Tsai, K.; Iwasawa, Y. *Chem. Lett.* **1996**, 755.
(12) Lin, J.-N.; Wan, B.-Z. *Appl. Catal. B* **2003**, *41*, 85.
(13) Fierro-Gonzalez, J. C.; Gates, B. C. *J. Phys. Chem. B* **2004**, *108*, 16999.
(14) Guzman, J.; Gates, B. C. *J. Phys. Chem. B* **2003**, *107*, 2242.
(15) Horváth, D.; Polisset-Thfoin, M.; Fraissard, J.; Guczi, L. *Solid State Ionics* **2001**, *131*, 153.
(16) Riahi, G.; Guillemot, D.; Polisset-Thfoin, M.; Khodadadi, A. A.; Fraissard, J. *Catal. Today* **2002**, *72*, 115.
(17) Guillemot, D.; Polisset-Thfoin, M.; Fraissard, J. *Catal. Lett.* **1996**, *41*, 143.
(18) Salama, T. M.; Shido, T.; Minagawa, H.; Ichikawa, M. *J. Catal.* **1995**, *152*, 322.
(19) Salama, T. M.; Ohnishi, R.; Shido, T.; Ichikawa, M. *J. Catal.* **1996**, *162*, 169.
(20) Van Zon, J. B.; Koningsberger, D. C.; Van Blik, H. F. J.; Sayers, D. E. *J. Phys. Chem.* **1985**, *82*, 5742.
(21) Boccuzzi, F.; Chiorino, A.; Manzoli, M.; Andreeva, D.; Tabakova, T. *J. Catal.* **1999**, *188*, 176.
(22) Daniells, S. T.; Overweg, A. R.; Makkee, M.; Moulijin, J. A. *J. Catal.* **2005**, *299*, 586.
(23) Boccuzzi, F.; Chiorino, A.; Tsubota, S.; Haruta, M. *J. Phys. Chem.* **1996**, *100*, 3625.
(24) Bollinger, M. A.; Vannice, M. A. *Appl. Catal. B* **1996**, *8*, 417.

(25) Schumacher, B.; Denkwitz, Y.; Plzak, V.; Kinne, M.; Behm, R. J. *J. Catal.* **2004**, *224*, 449.
(26) Lee, J. Y.; Schwank, J. *J. Catal.* **1986**, *102*, 207.
(27) Knell, A.; Barnickel, P.; Baiker, A.; Wolaun, A. *J. Catal.* **1992**, *137*, 306.
(28) Bollinger, M. A.; Vannice, M. A. *Appl. Catal. B* **1996**, *8*, 417.
(29) Lee, J. Y.; Schwank, J. *J. Catal.* **1986**, *102*, 207.
(30) Qui, S.; Ohnishi, R.; Ichikawa, M. *J. Phys. Chem. B* **1994**, *98*, 2719.
(31) Salama, T. M.; Ohnishi, R.; Ichikawa, M. *J. Chem. Soc., Faraday Trans.* **1996**, *92*, 301.
(32) Boccuzzi, F.; Chiorino, A.; Manzoli, M. *Surf. Sci.* **2000**, *942*, 454.
(33) Catana, G.; Baetens, D.; Mommaerts, T.; Schoonheydt, R. A.; Wackhuysen, B. M. *J. Phys. Chem. B* **2001**, *155*, 4904.
(34) Guillemot, D.; Borovkov, V. Yu.; Kazansky, V. B.; Polisset-Thfoin, M.; Fraissard, J. *J. Chem. Soc., Faraday Trans.* **1997**, *93*, 3587.
(35) Chang, C.-K.; Chen, Y.-J.; Yeh, C.-T. *Appl. Catal. A* **1998**, *174*, 13.
(36) Venugopal, A.; Scurrell, M. S. *Appl. Catal. A* **2004**, *258*, 241.
(37) Benfield, R. E.; Grandjean, D.; Kroll, M.; Pugin, R.; Sawitowski, T.; Schmid, G. *J. Phys. Chem. B* **2001**, *105*, 1961.
(38) Hardeveld, R. V.; Hartog, F. *Surf. Sci.* **1969**, *15*, 189.
(39) Bamwenda, G. R.; Tsubota, S.; Nakamura, T.; Haruta, M. *Catal. Lett.* **1997**, *44*, 83.
(40) Valden, M.; Lai, X.; Goodman, D. W. *Science* **1998**, *281*, 1647.
(41) Horch, S.; Lorensen, H. T.; Helveg, S.; Laegsgaard, E.; Stensgaard, I.; Jacobsen, K. W.; Norskov, J. K.; Bessenbacher, F. *Nature* **1999**, *398*, 134.
(42) Riahi, G.; Guillemot, D.; Polisset-Thfoin, M.; Bonnin, D.; Fraissard, J. *Stud. Surf. Sci. Catal.* **2001**, *135*, 11-O-01.
(43) Lin, J.-N.; Chen, J.-H.; Hsiao, C.-Y.; Kang, Y.-M.; Wan, B.-Z. *Appl. Catal. B* **2002**, *36*, 19.
(44) Kozlov, A. I.; Kozlova, A. P.; Liu, H.; Iwasawa, Y. *Appl. Catal. A* **1999**, *182*, 9.
(45) Okumura, K.; Yoshimoto, R.; Uruga, T.; Tanida, H.; Kato, K.; Yokota S.; Niwa, M. *J. Phys. Chem. B* **2004**, *108*, 6250.